Journal of Molecular Graphics and Modelling 28 (2010) 814–819

Contents lists available at ScienceDirect

Journal of Molecular Graphics and Modelling

journal homepage: www.elsevier.com/locate/JMGM

H-NOX domains display different tunnel systems for ligand migration

Yuebin Zhang, Ming Lu, Yingkun Cheng, Zhengqiang Li*

Key Laboratory for Molecular Enzymology and Engineering of the Ministry of Education, Jilin University, No. 2519 Jiefang Road, ChangChun 130021, Jilin Province, PR China

ARTICLE INFO

Article history:
Received 16 August 2009
Received in revised form 25 February 2010
Accepted 25 February 2010
Available online 3 March 2010

Keywords:
Hemoprotein
Ligand discrimination
sGC
LESMD
Multiple sequence alignment
H-NOX domain

ABSTRACT

Soluble guanylate cyclase (sGC) displays a high affinity for its physiological ligand (NO), but the ability of O_2 binding is not identified even if the presence of a large excess O_2 in vivo. Therefore, discrimination against O_2 by sGC is essential for NO signaling. Recently, the heme domain of sGC was termed as a member of new conversed hemoprotein family, namely H-NOX domain. Various ligand binding properties of H-NOX domains were observed and some of them bind O_2 tightly, whereas others have a poor affinity for O_2 or even no measurable affinity for O_2 at all like sGC. Several crystal structures of H-NOX domains are available now in both NO-bound form (Ns H-NOX; PDBid 2O0C) and O_2-bound form (Tt N-NOX; PDBid 1U55). These structures provide an ideal data for elucidating the molecular detail of ligand discrimination in H-NOX domains. In this work, by employing the locally enhanced sampling molecular dynamics (LESMD) simulations, we compared the ligand migration pathways between Ns H-NOX and Tt H-NOX. Interestingly, although they are similar in fold, the different spatial distributions of ligands between Ns H-NOX and Tt H-NOX are explored and proposed for ligand discrimination. The residue at position M144 in Ns H-NOX plays a key role in controlling the ligand entry and escape. However, in Tt H-NOX, the same position is a hydrogen-bonding tyrosine for stabilizing the oxygen binding and its steric effects of blocking the ligand migration is remarkable.

1. Introduction

Soluble guanylyl cyclase (sGC), the primary physiological receptor for nitric oxide (NO) in eukaryotes, is signal-transducing enzyme which catalyzes the conversion of GTP to cGMP [1]. The mammalian sGC is a heterodimer composed of two subunits (α/β) and a ferrous heme group function as the diatomic ligand sensor localizes to the N-terminal 194 amino acids of β subunit coordinated by His105 [2–5]. Both NO and CO can bind to the heme moiety of sGC readily but the molecular oxygen is excluded. As the native activator, NO binds to the iron atom of heme results in the conformational change of the enzyme from a transient six-coordinated low-spin state into a five-coordinated high-spin state therefore leads to a ~200–400 fold activation of sGC [6]. In contrast with NO, CO has a marginal activation effect (~4–6 fold compared to its basal activity) while only hexacoordination heme state is observed in CO-bound sGC [7]. However, in the presence of YC-1, sGC displays a robust activity stimulated by CO in vitro and five-coordinate CO-bound sGC is identified by resonance Raman spectroscopy [8,9].

Recently, Iyer et al. identified that the sGC heme domain was a member of a highly conserved family of hemoproteins [10], named H-NOX domain (heme-nitric oxide or OXygen-binding domain) [11]. Several crystal structures of H-NOX domains are available now whereas the structure of sGC is not solved yet [12–14]. In 2004, Marletta group reported the first crystal structure of the H-NOX domain from *Thermoanaerobacter tengcongensis* (Tt H-NOX) which forms a stable O_2-bound form and shares 18% sequence identity with sGC [14]. The heme is coordinated by His102 and the invariant Y × S × R motif is involved in hydrogen bonding interaction with the heme propionate group in Tt H-NOX [14,15]. Moreover, the residue Y140 has been found to play a key role in stabilizing the O_2 binding [16]. In 2007, Ma et al. reported the crystal structures of the H-NOX domain from Nostoc sp. (Ns H-NOX) in ligand free, NO-bound, and CO-bound forms [12]. Ns H-NOX has a much higher sequence identity (33% identity) with sGC compared to Tt H-NOX and demonstrates a higher degree of similarity among the residues which define the distal heme pocket.

Discrimination against O_2 by sGC is remarkable and important for NO signaling because the concentration of O_2 is much higher than that of NO in vivo. The crystal structure of O_2-bound Tt H-NOX shed new light on the ligand discrimination between NO and O_2 [14], but it is still far from fully elucidating the mechanisms of ligand discrimination in H-NOX domains especially in sGC. As mentioned above, the Tyr140 in distal pocket is crucial for O_2 binding in Tt H-NOX [16]. Mutating Tyr140 to an hydrophobic residue (Y140L) increases the rate of O_2 dissociation and consequently does not form a stable O_2-bound complex [16]. However, converting Ile 145 to Tyr at the same position in full-length sGC was found not

* Corresponding author. Tel.: +86 431 88499261; fax: +86 431 88980440.
E-mail address: lzq@jlu.edu.cn (Z. Li).

1093-3263/$ – see front matter © 2010 Elsevier Inc. All rights reserved.
doi:10.1016/j.jmgm.2010.02.007

to bind O_2 [17]. Moreover, the binding and dissociation of NO and CO are also impeded in I145Y mutant sGC [18]. Obviously, putting the focus on the distal heme pocket environment alone would not provide sufficient evidence to clarify the mechanisms of ligand discrimination in H-NOX domains.

In this article, we present a theoretical study by employing the locally enhanced sampling molecular dynamics (LESMD) to explore the ligand migration pathways in H-NOX proteins [19,20]. Surprisingly, distinct pathways for ligand migrating are observed between the Ns H-NOX and Tt H-NOX though they are similar in fold (see Fig. 1). These results would propose a reasonable explanation for the mechanisms of ligand recognition in H-NOX domains at atomic level.

2. Materials and methods

2.1. Locally enhanced sampling molecular dynamics (LESMD)

LESMD is an effective way to identify the tunnel systems by using a mean field approach enhancing the sampling of the conformational space due to the presence of multiple copies of ligand [19]. Initially, multiple copies of ligands are settled together with the same coordinates, for example of 15 copies at the distal binding cavity. During the simulation, the copies are free to move apart in a way of neglecting their interaction of each other but considering the interaction with the rest of the system in an average way and explore different regions of conformational space in the protein matrix. High energy barriers may be caused by steric conflicts or other unfavorable interactions. However, the rest of the system will adjust each of these 15 copies with a scaling factor of 1/15. In a LES systems, more frequent conformational changes will be observed due to the reduced barriers to conformational transitions comparing to the original system [19]. If one copy is in an unfavorable conformation, the others may not be, and the effective barriers with a distribution of copies are less than with the single copy. To sum up, the major advantage of LES is that multiple patterns of ligand distribution in protein matrix can be obtained by means of increasing the statistical sampling when only perform a single simulation.

2.2. Preparation of the systems

The Ns and Tt H-NOX domain structures were obtained from Protein Data Bank (PDB code 1U55 and 2O0G respectively; chain A). In order to mimic the photodissociated CO migration process, the oxygen molecule in Tt H-NOX was replaced by carbon monoxide and the Fe–C–O angle was adjusted to above 160° in silico then the CO–Fe bond was cut for both of the equilibrated structures. The VMD [21] molecular graphic program was used to prepare the structure for LESMD simulation. The two structures were solvated in a TIP3P water box (9188 waters with dimension 76 Å × 43 Å × 44 Å for Tt H-NOX; 9250 waters with dimension 49 Å × 49 Å × 59 Å for Ns H-NOX) and 0.5 mol/L NaCl was added each to make the whole system chargeless. Fifteen copies of CO molecules were inserted using the multiply command in VMD.

2.3. MD simulation

Locally enhanced sampling molecular dynamics calculations were carried out using NAMD2.6 [22] program and the CHARMM27 force field [23]. Parametrization of CO was taken from CHARMM27 force field (ε = −0.11 kcal/mol, *R*min/2 = 2.1 Å, lbond = 1.13 Å) [24]. Simulations were performed with periodic boundary conditions. The particle mesh Ewald method was used for the calculation of the long-range interactions. The van der Waals and electrostatic interactions were calculated within a cutoff of 12 Å. The switch distance was 10 Å, and 1.0 1–4 scaling factor was used. The step size was set at 2 fs with the rigid bonds parameter activated.

All systems were minimized with the backbone fixed for 5000 steps and then all atoms were minimized for another 5000 steps using the conjugate gradient algorithm. Heating of the systems were performed from 10 to 310 K during the next 30,000 steps in 10-K increments. The volume was then equilibrated for 10,000 steps by turning the Langevin piston on. Finally both of the systems were equilibrated in the NPT ensemble (310 K and 1 atm) for 30,000 steps. Then a 10 ns MD simulation runs were performed at constant volume and temperature each for the LESMD analysis.

The volume of the gap regions was calculated using SURFNET program [25] with a grid separation of 0.8 Å and a minimum and maximum gap sphere radius of 1.0 and 3.0 Å, respectively. The Gromacs [26] tools and VMD [21] scripts were used to analyse all the MD trajectories. The contact collision was counted within a distance of 4 Å between the ligand and the protein heavy atom [19].

3. Results and discussion

3.1. Structural and dynamical comparison between Ns H-NOX and Tt H-NOX

The H-NOX domains consist of seven α-helices (named αA–G), and one four-stranded antiparallel β-sheet (named β1–4; Fig. 1(a)). The folding state of H-NOX domains is new and has no significant similarity comparing with previously characterized hemoproteins. To test the stability of the two H-NOX domains, we calculated the root mean square deviation (RMSD) of the backbone atoms during our 10 ns simulation. As can be seen in Fig. 1(b), The Tt H-NOX experienced an uneven change in deviation. The RMSD of Tt H-NOX fluctuate a lot between 1 and 2.5 Å and comparing to its root mean square fluctuation (RMSF) plots indicate that the primary contribution to the fluctuation come from the regions of residue 102–115 with two peaks at residue 107 and 110. Looking back to the structure, the higher mobility sequence locates at αFβ1 loop of Tt H-NOX and moreover it is the key region that connects the distal and proximal area of heme group. The structural fluctuations are consistent with the previously reported simulations by Capece et al. [27]. In contrast, the RMSD of Ns H-NOX is more stable than that of Tt H-NOX and the only noticeable displacements were found in the regions of β3β4 loop around residue 169. Note that the same behavior was also observed in the Tt H-NOX but with a small RMSF value of that region.

3.2. Ns H-NOX domain ligand migration pathway

During the 10 ns LESMD simulations, a two branched ligand migration pathway has been identified in Ns H-NOX domain shown in Fig. 2(a) and (b). In addition, a much quicker ligands migration rate was observed in Ns H-NOX owing to a large cavity volume of distal heme pocket and lacking the hydrogen bond network, this will be discussed later. In the first 170 ps, all ligands diffused out of the distal heme pocket and the first ligand began to escape into the solvent through the short tunnel system. After 700 ps, 12 of the ligands left in the interior of the protein and 5 of them located in the long tunnel. At 1.12 ns of the trajectory, only one of the ligands remained in the protein matrix and 10 of them gathered at the portal of the short tunnel. In the next 200 ps, four ligands overcame the energy barrier and exited into the solvent while others reentered into the tunnel. Throughout the 10 ns trajectory, 12 of the ligands migrated escaped using the short tunnel while only 2 of the ligands exited via the long tunnel branch. One of the ligands remained in the protein after the 10 ns simulations.

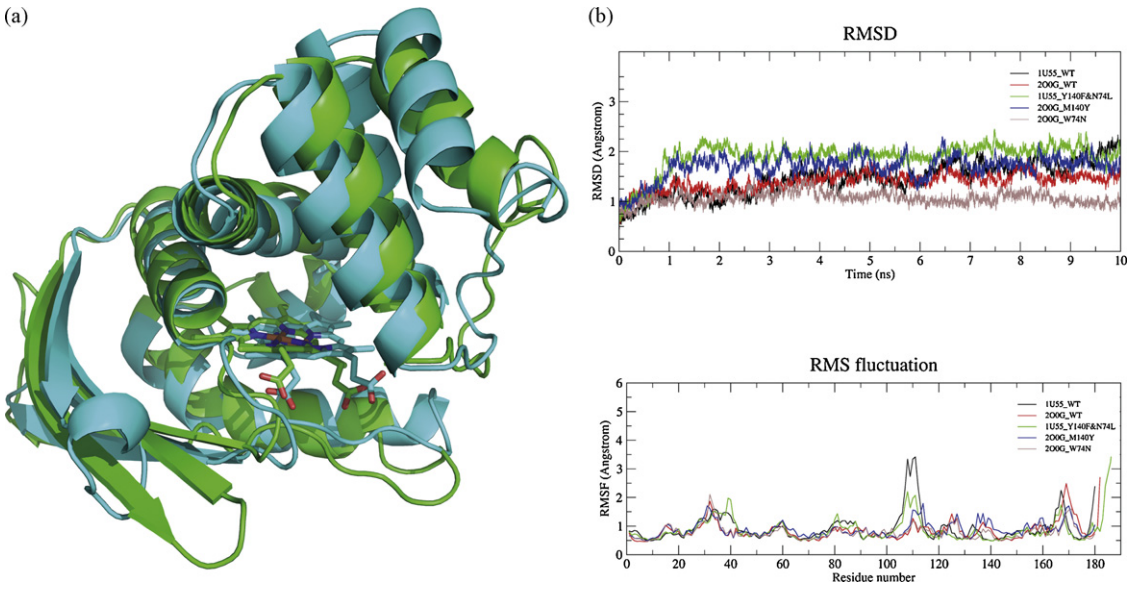

Fig. 1. (a) Structural alignment of H-NOX domains form Ns (cyan, PDBid 2O0G monomer A) and Tt (green, PDBid 1U55 monomer A). The RMS between the two backbone structures is 2.15 Å. The figure was rendered using PyMOL [31]. (b) Backbone RMSD (top) and RMSF vs residue (bottom).

3.3. *Tt H-NOX domain ligand migration pathway*

During our simulations, only one migration path was explored in Tt H-NOX domain (Fig. 2(c) and (d)). Interestingly, the tunnel system hosted in Tt H-NOX faced a different direction compared to that observed in Ns H-NOX domain. Before 2 ns, all ligands were trapped in the distal heme pocket of Tt H-NOX defined by ILE5, TRP9, ASN74, PHE78, TYR140 and LEU144. It was until 2.37 ns, concomitant with a movement of αfβ1 loop region (see Fig. 1(b) and Supporting Information), the first ligand began to exit out of the distal pocket into the next cavity. This indicates that a lower ligand migration rate would be expected in WT Tt H-NOX domain and the results are in accordance with the experimental data [16]. Another prominent feature of Tt H-NOX domain is that, at 2.5 ns of the simu-

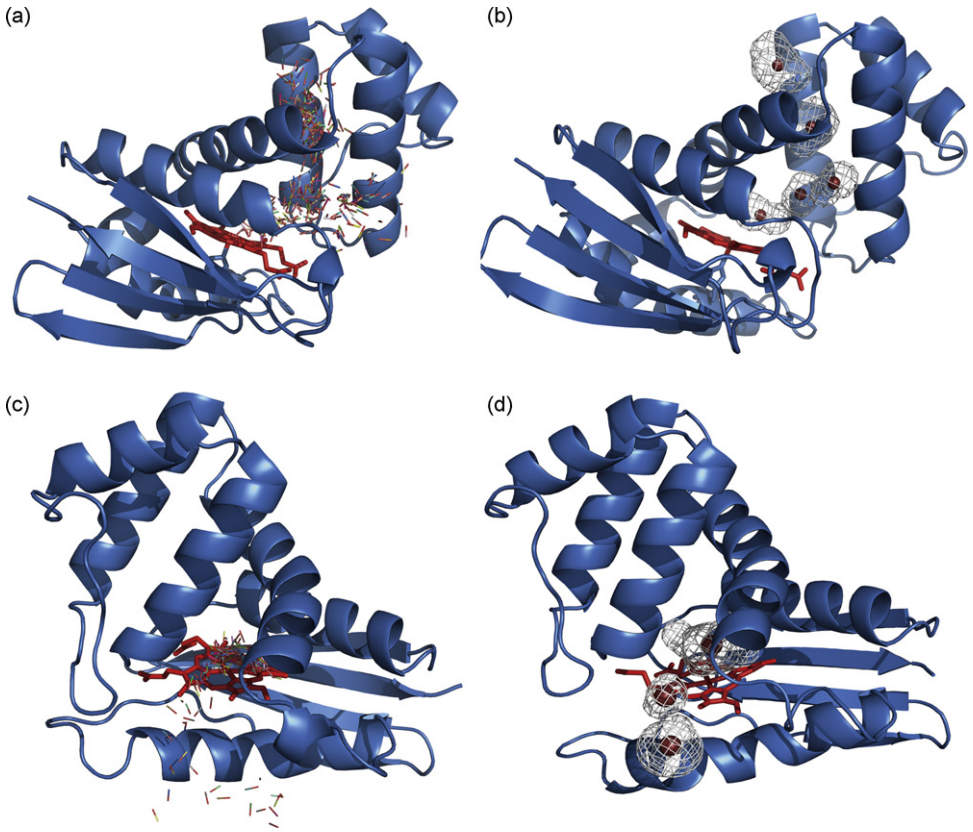

Fig. 2. The results of LESMD simulation of the Ns H-NOX (a) and Tt H-NOX (c). The proteins are shown as cartoon in skyblue and the heme group is shown as stick in red. The colorful sticks are the selected ligands to represent those spatial distributions in Ns H-NOX (a) and Tt H-NOX (c). The SURFNET program [25] was employed to portray the cavity systems of ligand migration pathways in Ns H-NOX (b) and Tt H-NOX (d).

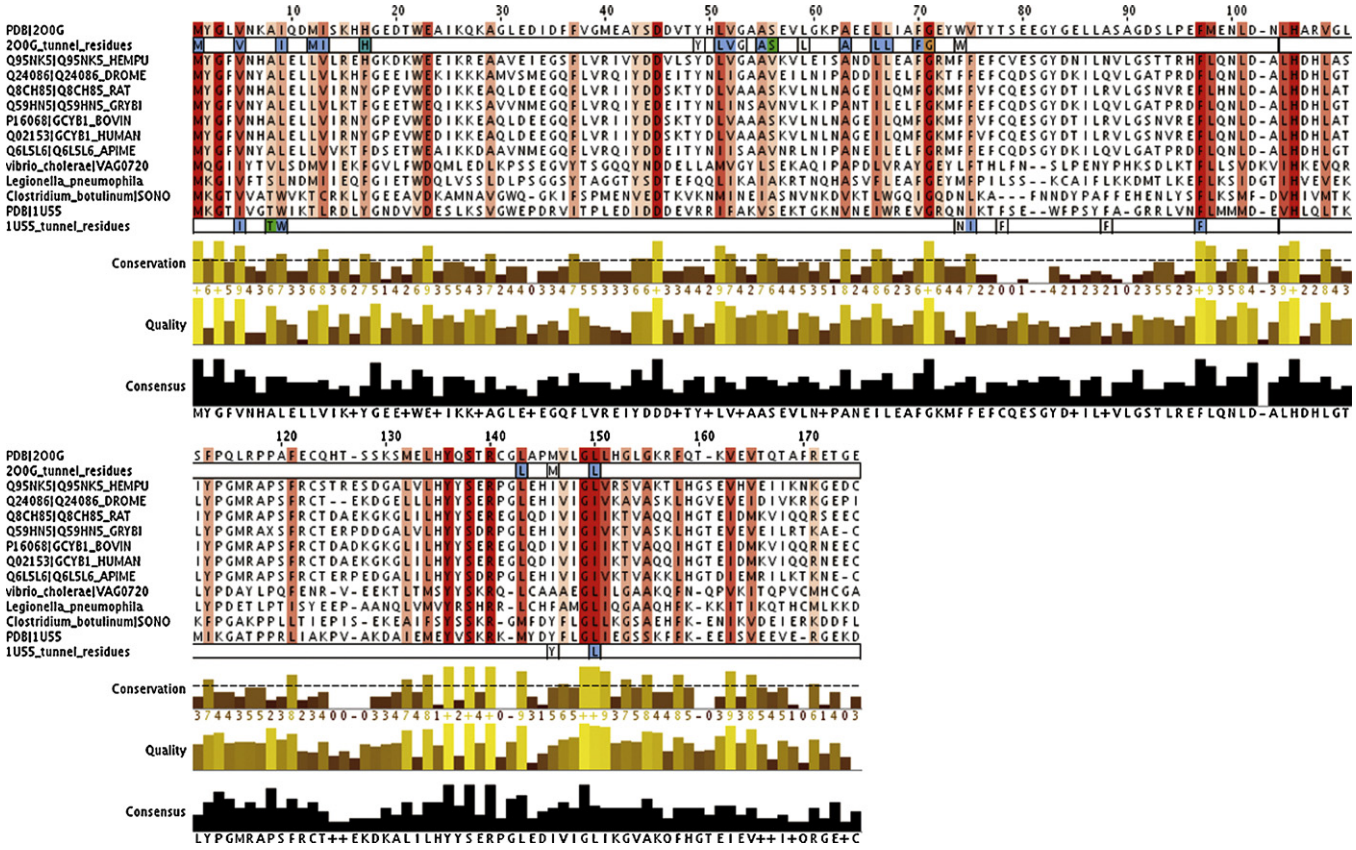

Fig. 3. The sequence alignment of selects H-NOX domains. The second row and the last row of the alignment represent the key residues lining the tunnel system in Ns H-NOX and Tt H-NOX respectively. These residues were identified by the collision counts. The H-NOX proteins share a very strong amino acid sequence identity at the position which defines the tunnel systems. The multiple sequence alignment was generated using Jalview [32].

lations, CO migrated into the proximal side of the heme group from distal heme pocket via a temporary cavity. The similar migration process was also observed in myoglobin by using time-resolved crystallography and molecular dynamics simulations [28,29] but not identified in Ns H-NOX in present study because of the different orientations of the tunnel system between the two proteins. At the end of the 10 ns simulation runs, three of the ligands remained in the interior of the protein.

3.4. Ligand discrimination mechanism between Ns H-NOX and Tt H-NOX

The size of the distal pocket has a critical impact on the rate of ligand entry and escape [30]. The key amino acids in the distal pocket are quite different between the two proteins and Tt H-NOX has a smaller volume of DP compared to Ns H-NOX (see Fig. 2). Despite the distal hydrogen-bond effects, the mutation of Tyr140 to Leu in Tt H-NOX would enlarge the distal pocket, increase the geminate rebinding process and impact the formation of a stable O_2 complex. On the other hand, introducing a Tyr at the position 145 (I145Y) in the fragment 1–385 of sGC beta1 subunit showed a extremely low oxygen association rate [16], indicated that altering the distal pocket environment by affording the hydrogen-bond network and decreasing the volume size of the distal cavity affect the ligand binding property of sGC indeed. As mentioned in Section 1, the I145Y mutation in the full-length beta-subunit of the sGC heterodimer did not have the capacity to bind O_2 [17,18]. These results suggest that this mutant is an inappropriate mimic of its oxygen binding property.

We are inclined to propose that the different protein matrix tunnel systems between Ns H-NOX and Tt H-NOX lead to these incomprehensible results. As shown in Figs. 3 and 4, the residues in the distal pocket not only define the heme environment but also determine the direction of ligands migration in our simulations. In

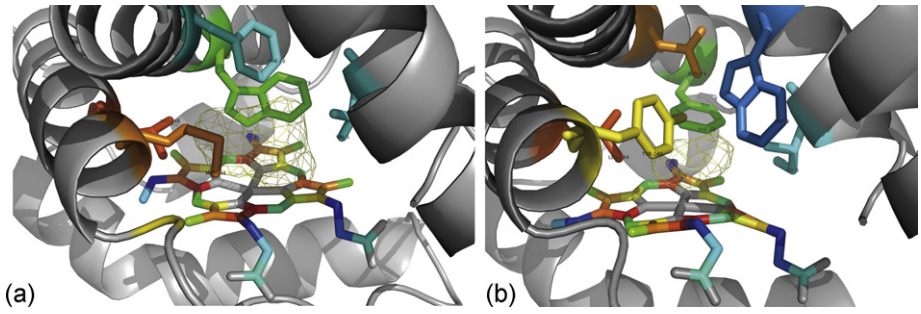

Fig. 4. The key residues define the distal heme pocket of Ns H-NOX (a) and Tt H-NOX (b). The distal pocket volume is 75 Å^3 in Ns H-NOX and 21 Å^3 in Tt H-NOX respectively.

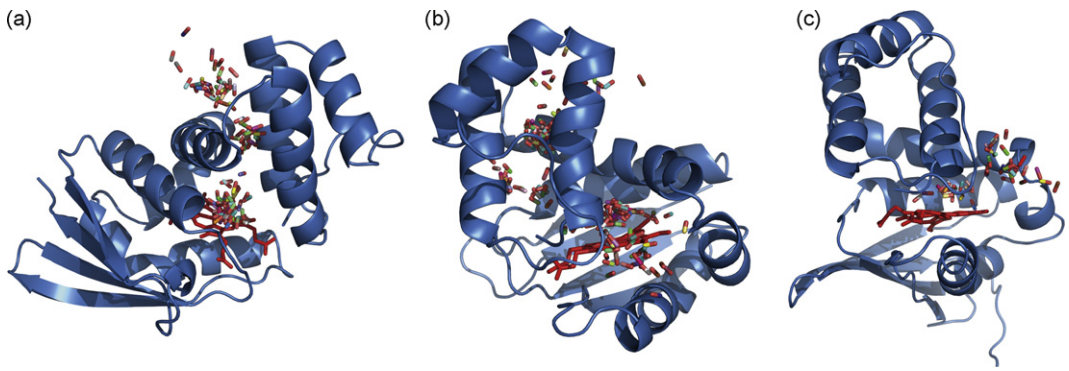

Fig. 5. The selected ligand distributions of 10 ns simulations in M144Y Ns H-NOX (a), W74N Ns H-NOX (b) and Y140F&N74L Tt H-NOX (c) respectively.

Ns H-NOX, the indole ring of W74 is perpendicular to the heme plan and forms a very strong steric hindrance preventing the ligands migration whereas the residue at the same position is F in sGC and N in Tt H-NOX respectively. On the contrary, in Tt H-NOX, Tyr140, Asn74 and Trp9 are involved in forming a three-dimensional hydrogen bond networks blocking the ligand migration which are absent from the H-NOX domains of facultative aerobes and vertebrate sGCs [11]. Therefore, the different spatial distributions of ligands between Ns H-NOX and Tt H-NOX are observed in present work (see Fig. 3). Most importantly, in the H-NOX domains which cannot bind O_2, a direct result of introducing the Tyr to the heme pocket (the residue is M144 in Ns H-NOX and I145 in sGC at this position) is the effect of blocking ligands migration. The mutation would separate the adjacent cavities with little connection (Fig. 2(b)), hence the ligand binding properties of the I145Y sGC mutant were impaired [16–18].

3.5. *In silico mutation studies of Ns and Tt H-NOX domain*

As mentioned above, we proposed that several crucial residues played key roles in controlling the ligand migration process. In order to test these hypotheses, three mutation LESMD studies were performed in this work: (I) introducing a Tyr into the heme pocket at M144 in Ns H-NOX; (II) mutating W74 to N in Ns H-NOX; (III) a dual mutation Y140F&N74L in Tt H-NOX to eliminate the side chain hydrogen-bonding effects in the heme pocket.

As shown in Fig. 5(a), only the long branch tunnel was observed in the M144Y Ns H-NOX, the Tyr at position 144 in Ns H-NOX blocked the ligand migration from the short branch tunnel. In this case, a very low ligand migration rate was identified in the M144Y Ns H-NOX compared to that in the WT Ns H-NOX, due to lacking one of the ligand migration pathways. After 10 ns LESMD simulations in M144Y Ns H-NOX, eight ligand still confined in the heme pocket.

As expected in the W74N Ns H-NOX LESMD simulation, a total of three ligand migration pathways were explored (Fig. 5(b)). Mutating the tryptophan to asparagine in Ns H-NOX opened a new branch of ligand migration pathways which only existed in the WT Tt H-NOX (Fig. 2(c)). During the 10 ns simulation, all ligands had escaped out of the protein matrix. Moreover, most of the ligands (8/15) came out from the new branch pathway whereas three of ligands escaped from the short pathway and four of ligands migrated via the long branch tunnel.

The dual mutation Y140F&N74L in Tt H-NOX did not alter the ligand migration pathways as shown in Fig. 5(c) but a very fast ligand migration process occurred. As mentioned previously, the ligands restricted in the heme pocket of the WT Tt H-NOX nearly 3 ns before they migrated out of the protein, but when we eliminated the side chain hydrogen-bonding effects by mutating the Y140F&N74L in Tt H-NOX, the ligands spread out immediately in the heme pocket and at 800 ps the first ligand began to escape out of the protein. At the end of the 10 ns simulation, 14/15 ligands had migrated out of the protein except one still in the heme pocket.

4. Conclusions

In present simulations, the different ligand migration patterns were observed between the NO-bound H-NOX domain (Ns H-NOX) and O_2-bound H-NOX domain (Tt H-NOX) and the different volume sizes of distal pocket between them were also identified because of the differences in residue composition. The residue at position 144 in Ns H-NOX plays a key role in modulating the process of the ligand migration whereas, in Tt H-NOX, the ligands migrate toward other direction owning to the steric effects and the hydrogen bond networks at the site. These results can give a new insight into explaining the molecular mechanism of ligand discrimination in H-NOX family.

Acknowledgement

Fund was supported by the National Natural Science Foundation of China (30570404, 30670458).

Appendix A. Supplementary data

Supplementary data associated with this article can be found, in the online version, at doi:10.1016/j.jmgm.2010.02.007.

References

[1] H.H. Schmidt, S.M. Lohmann, U. Walter, The nitric oxide and cGMP signal transduction system: regulation and mechanism of action, Biochim. Biophys. Acta 1178 (1993) 153–175.
[2] B. Wedel, P. Humbert, C. Harteneck, J. Foerster, J. Malkewitz, E. Bohme, G. Schultz, D. Koesling, Mutation of His-105 in the beta 1 subunit yields a nitric oxide-insensitive form of soluble guanylyl cyclase, Proc. Natl. Acad. Sci. U.S.A. 91 (1994) 2592–2596.
[3] A.J. Hobbs, L.J. Ignarro, Nitric oxide–cyclic GMP signal transduction system, Methods Enzymol. 269 (1996) 134–148.
[4] Y. Zhao, J.P. Schelvis, G.T. Babcock, M.A. Marletta, Identification of histidine 105 in the beta1 subunit of soluble guanylate cyclase as the heme proximal ligand, Biochemistry 37 (1998) 4502–4509.
[5] D.S. Karow, D. Pan, J.H. Davis, S. Behrends, R.A. Mathies, M.A. Marletta, Characterization of functional heme domains from soluble guanylate cyclase, Biochemistry 44 (2005) 16266–16274.
[6] T.L. Poulos, Soluble guanylate cyclase, Curr. Opin. Struct. Biol. 16 (2006) 736–743.
[7] G. Deinum, J.R. Stone, G.T. Babcock, M.A. Marletta, Binding of nitric oxide and carbon monoxide to soluble guanylate cyclase as observed with resonance Raman spectroscopy, Biochemistry 35 (1996) 1540–1547.
[8] Z. Li, B. Pal, S. Takenaka, S. Tsuyama, T. Kitagawa, Resonance Raman evidence for the presence of two heme pocket conformations with varied activities in CO-bound bovine soluble guanylate cyclase and their conversion, Biochemistry 44 (2005) 939–946.

[9] B. Pal, T. Kitagawa, Interactions of soluble guanylate cyclase with diatomics as probed by resonance Raman spectroscopy, J. Inorg. Biochem. 99 (2005) 267–279.
[10] L.M. Iyer, V. Anantharaman, L. Aravind, Ancient conserved domains shared by animal soluble guanylyl cyclases and bacterial signaling proteins, BMC Genomics 4 (2003) 5.
[11] E.M. Boon, M.A. Marletta, Ligand discrimination in soluble guanylate cyclase and the H-NOX family of heme sensor proteins, Curr. Opin. Chem. Biol. 9 (2005) 441–446.
[12] X. Ma, N. Sayed, A. Beuve, F. van den Akker, NO and CO differentially activate soluble guanylyl cyclase via a heme pivot-bend mechanism, EMBO J. 26 (2007) 578–588.
[13] P. Nioche, V. Berka, J. Vipond, N. Minton, A.L. Tsai, C.S. Raman, Femtomolar sensitivity of a NO sensor from *Clostridium botulinum*, Science 306 (2004) 1550–1553.
[14] P. Pellicena, D.S. Karow, E.M. Boon, M.A. Marletta, J. Kuriyan, Crystal structure of an oxygen-binding heme domain related to soluble guanylate cyclases, Proc. Natl. Acad. Sci. U.S.A. 101 (2004) 12854–12859.
[15] P.M. Schmidt, M. Schramm, H. Schroder, F. Wunder, J.P. Stasch, Identification of residues crucially involved in the binding of the heme moiety of soluble guanylate cyclase, J. Biol. Chem. 279 (2004) 3025–3032.
[16] E.M. Boon, S.H. Huang, M.A. Marletta, A molecular basis for NO selectivity in soluble guanylate cyclase, Nat. Chem. Biol. 1 (2005) 53–59.
[17] C. Rothkegel, P.M. Schmidt, F. Stoll, H. Schroder, H.H. Schmidt, J.P. Stasch, Identification of residues crucially involved in soluble guanylate cyclase activation, FEBS Lett. 580 (2006) 4205–4213.
[18] E. Martin, V. Berka, E. Bogatenkova, F. Murad, A.L. Tsai, Ligand selectivity of soluble guanylyl cyclase: effect of the hydrogen-bonding tyrosine in the distal heme pocket on binding of oxygen, nitric oxide, and carbon monoxide, J. Biol. Chem. 281 (2006) 27836–27845.
[19] R. Elber, M. Karplus, Enhanced sampling in molecular dynamics: use of the time-dependent Hartree approximation for a simulation of carbon monoxide diffusion through myoglobin, J. Am. Chem. Soc. 112 (1990) 9161–9175.
[20] S.D. Golden, K.W. Olsen, Identification of ligand-binding pathways in truncated hemoglobins using locally enhanced sampling molecular dynamics, Methods Enzymol. 437 (2008) 459–475.
[21] W. Humphrey, A. Dalke, K. Schulten, VMD: visual molecular dynamics, J. Mol. Graph. 14 (1996), 33–38, 27–38.
[22] J.C. Phillips, R. Braun, W. Wang, J. Gumbart, E. Tajkhorshid, E. Villa, C. Chipot, R.D. Skeel, L. Kale, K. Schulten, Scalable molecular dynamics with NAMD, J. Comput. Chem. 26 (2005) 1781–1802.
[23] D. Bashford, Bellott, R.L. Dunbrack, J.D. Evanseck, M.J. Field, S. Fischer, J. Gao, H. Guo, S. Ha, D. Joseph-McCarthy, L. Kuchnir, K. Kuczera, F.T.K. Lau, C. Mattos, S. Michnick, T. Ngo, D.T. Nguyen, B. Prodhom, W.E. Reiher, B. Roux, M. Schlenkrich, J.C. Smith, R. Stote, J. Straub, M. Watanabe, J. Wiorkiewicz-Kuczera, D. Yin, M. Karplus, All-atom empirical potential for molecular modeling and dynamics studies of proteins, J. Phys. Chem. B 102 (1998) 3586–3616.
[24] J. Cohen, A. Arkhipov, R. Braun, K. Schulten, Imaging the migration pathways for O_2, CO, NO, and Xe inside myoglobin, Biophys. J. 91 (2006) 1844–1857.
[25] R.A. Laskowski, SURFNET: a program for visualizing molecular surfaces, cavities, and intermolecular interactions, J. Mol. Graph. 13 (1995), 323–330, 307–328.
[26] D. Van Der Spoel, E. Lindahl, B. Hess, G. Groenhof, A.E. Mark, H.J. Berendsen, GROMACS: fast, flexible, and free, J. Comput. Chem. 26 (2005) 1701–1718.
[27] L. Capece, D.A. Estrin, M.A. Marti, Dynamical characterization of the heme NO oxygen binding (HNOX) domain. Insight into soluble guanylate cyclase allosteric transition, Biochemistry 47 (2008) 9416–9427.
[28] J.Z. Ruscio, D. Kumar, M. Shukla, M.G. Prisant, T.M. Murali, A.V. Onufriev, Atomic level computational identification of ligand migration pathways between solvent and binding site in myoglobin, Proc. Natl. Acad. Sci. U.S.A. 105 (2008) 9204–9209.
[29] A. Tomita, T. Sato, K. Ichiyanagi, S. Nozawa, H. Ichikawa, M. Chollet, F. Kawai, S.Y. Park, T. Tsuduki, T. Yamato, S.Y. Koshihara, S. Adachi, Visualizing breathing motion of internal cavities in concert with ligand migration in myoglobin, Proc. Natl. Acad. Sci. U.S.A. 106 (2009) 2612–2616.
[30] E.E. Scott, Q.H. Gibson, J.S. Olson, Mapping the pathways for O_2 entry into and exit from myoglobin, J. Biol. Chem. 276 (2001) 5177–5188.
[31] W.L. DeLano, The PyMOL Molecular Graphics System, DeLano Scientific, San Carlos, CA, USA, 2002.
[32] M. Clamp, J. Cuff, S.M. Searle, G.J. Barton, The Jalview Java alignment editor, Bioinformatics 20 (2004) 426–427.